Available online at www.sciencedirect.com
ScienceDirect
Cement and Concrete Research 36 (2006) 2021–2032
Cement and Concrete Research

Quantitative Rietveld analysis of CAC clinker phases using synchrotron radiation

F. Guirado [a,*], S. Galí [b]

[a] Servei de Recursos Científics i Tècnics, Univ. Rovira i Virgili, Campus Sescelades, Tarragona, Catalonia 43005, Spain
[b] Dep. Cristal·lografia, Univ. Barcelona, Martí i Franquès sn, Barcelona, Catalonia 08028, Spain

Received 3 May 2005; accepted 29 May 2006

Abstract

The quantitative Rietveld analyses of twenty samples of CAC from four different manufacturers over the world, one synthetic mixture and a NIST standard were performed using synchrotron radiation. As compared with conventional XRD, synchrotron powder diffraction permitted to find new minor phases, improve the characterization of solid solutions of iron rich CAC phases and reduce preferential orientation and microabsorption effects. Diffraction data were complemented with XRF and TG/DT analyses. Synchrotron results were used as a reference test to improve the performance of conventional powder diffraction, by an accurate selection of refinable profile and structural parameters, and permitted to extract several recommendations for conventional quantitative Rietveld procedures. It is shown that with these recommendations in mind, conventional XRD based Rietveld analyses are comparable to those obtained from synchrotron data. In summary, quantitative XRD Rietveld analysis is confirmed as an excellent tool for the CAC cement industry.

Keywords: Synchrotron diffraction; X-ray diffraction; Quantitative Rietveld analysis; Calcium aluminate cement

1. Introduction

Standardless Rietveld quantitative analysis of clinker phases is becoming a straightforward reliable tool for quality control in cement industry. In recent years several important papers on Rietveld analysis of both, Portland [1,2] and calcium aluminate (CAC) cements [3,4] have been published, drawing the attention on the potential advantages of the method, as compared with other traditional quantitative methods of the cement industry.

The quantitative Rietveld method is based on two premises: one is the accurate knowledge of the crystal structures of the phases present, and the other regards all the instrumental factors involved in the obtention of the diffraction profile. The knowledge of the structural variations expected in clinker phases allows a wise selection of the crystallographic parameters that can be introduced in the fitting model. On the other hand, the accurate calibration of the diffractometer permits to minimize the instrument dependent parameters used, avoiding misleading correlations between structural and instrumental parameters, that may introduce bias in the quantification of phases.

Since the cement is produced from natural or recycled raw materials with variable composition, the clinker produced results in a complex variable multiphase–multicomponent system. The full characterization of this system from a single powder diffraction profile requires the previous solution of several important problems. For CAC, a non-exhaustive list of these problems include: a) identification of minor phases (less than 2 wt.%) [5–7] b) identification of hydrated phases, c) characterization of the extent of solid solutions in major phases [8–10], d) knowledge of the influence of different absorption coefficients on quantitative results, e) deviations due to preferential orientation etc.

In the normal practice in industry or research, a conventional Bragg–Brentano X-ray powder diffractometer is likely to be used for routine identification and quantification work. These instruments, even if they are improving their performances, have inherent limitations due mainly to their source emission profile and limited intensity [11]. As a consequence, for multiphase samples, severe overlapping of diffracting peaks may introduce strong correlations between crystal to crystal and crystal to instrument

* Corresponding author. Tel.: +34 977 55 97 83; fax: +34 977 55 82 61.
E-mail address: francesc.guirado@urv.cat (F. Guirado).

0008-8846/$ - see front matter © 2006 Elsevier Ltd. All rights reserved.
doi:10.1016/j.cemconres.2006.05.019

Table 1
Weight percent of simple oxides obtained by XRF

Sample	CaO	Al_2O_3	Fe_2O_3	FeO	SiO_2	MgO	TiO_2	P_2O_5	K_2O	MnO	Na_2O	l.o.i.	Total
A1	38.12	39.32	9.90	3.24	2.84	0.44	1.61	0.03	0.05	0.01	0.00	1.65	97.20
A2	39.16	38.24	9.71	2.79	3.05	0.47	1.54	0.07	0.04	0.01	0.00	2.20	97.29
A3	37.00	40.78	10.70	2.79	2.90	0.42	1.69	0.07	0.02	0.01	0.00	1.25	97.63
A4	36.61	40.83	12.08	1.26	2.88	0.43	1.69	0.06	0.03	0.01	0.00	1.15	97.03
A5	37.35	40.96	10.59	2.70	2.75	0.43	1.70	0.07	0.02	0.01	0.00	0.89	97.47
A6	36.42	42.10	11.11	2.25	2.34	0.44	1.75	0.07	0.02	0.01	0.00	0.79	97.29
A7	36.14	41.59	10.67	2.70	2.69	0.44	1.75	0.08	0.02	0.01	0.00	1.16	97.25
A8	37.28	40.86	9.46	3.61	2.61	0.46	1.71	0.08	0.02	0.01	0.00	1.11	97.19
A9	36.74	41.10	9.25	4.60	2.88	0.46	1.73	0.08	0.02	0.01	0.00	0.72	97.59
A10	35.75	41.44	10.86	2.97	3.21	0.43	1.74	0.09	0.03	0.01	0.00	0.89	97.41
B1	37.18	39.15	11.92	1.44	3.21	0.24	1.60	0.04	0.04	0.02	0.00	1.68	96.51
C1	36.88	38.84	11.80	0.18	4.77	0.81	1.74	0.19	0.04	0.26	0.00	0.95	96.46
C2	35.93	51.22	1.55	0.00	4.93	0.36	1.99	0.08	0.29	0.02	0.00	1.45	97.80
C3	27.78	70.47	0.00	0.00	0.38	0.00	0.05	0.01	0.00	0.01	0.00	0.93	99.62
D1	25.70	72.86	0.00	0.00	0.16	0.00	0.02	0.00	0.00	0.01	0.01	0.61	99.36
D2	25.09	73.43	0.00	0.00	0.12	0.02	0.03	0.00	0.00	0.01	0.00	0.62	99.31
D3	16.88	81.12	0.00	0.00	0.13	0.00	0.03	0.00	0.00	0.01	0.17	1.37	99.70
D4	24.40	74.46	0.00	0.00	0.10	0.02	0.04	0.00	0.00	0.01	0.00	0.56	99.58
D5	25.25	73.48	0.00	0.00	0.11	0.00	0.03	0.00	0.00	0.01	0.00	0.78	99.65
D6	17.31	80.21	0.00	0.00	0.15	0.00	0.03	0.00	0.00	0.00	0.38	1.31	99.40

FeO was calculated from thermogravimetric data.
Zero values indicate amounts under detection limit.

parameters, depending on the number of phases and their symmetry. In addition, the absorption contrast between phases may give rise to a systematic underestimate of the more absorbing ones.

Synchrotron X-ray powder diffraction may help to overcome most of these drawbacks, allowing the validation or eventually the modification of the current procedures in conventional X-ray Rietveld quantitative analysis of CACs. The main advantages of a synchrotron source are high brilliance (higher flux of photons), very low spectral dispersion, small vertical divergence and higher energy (smaller radiation length) [12]. As a result, absorption effects are minimized, minor phases are made visible and the improved resolution reduce correlations between parameters, and improve accuracy.

In this paper the authors analyze twenty samples of CAC clinker from four different factories, plus one NIST standard and a synthetic mixture using synchrotron radiation powder diffraction. The characterization of the samples was complemented by XRF analysis, thermogravimetric and differential thermal analyses (TG/DTA). Finally, the samples were analyzed by conventional X-ray powder diffraction. The comparison of the quantitative results obtained with synchrotron and conventional X-ray, permits to find out the possibilities and intrinsic limitations of conventional powder diffraction, and to derive several recommendations for routine Rietveld quantitative phase analyses of CACs.

2. Experimental

2.1. Collecting of the samples

The authors contacted CAC producers all over the world to expose the project and solicit their collaboration. Four important

Table 2
Parameters used for quantitative analyses with synchrotron and conventional diffraction data and for iron rich and iron poor cement

	Synchrotron radiation diffraction		X-ray diffraction	
	Fe-rich cement	Fe-poor cement	Fe-rich cement	Fe-poor cement
Background (Chebychev coefficients)	9	8	6	6
Profile function	Pseudo-Voigt	Pseudo-Voigt	Fundamental parameters	Fundamental parameters
Cell parameters	Fitted for all phases	Fitted for all phases	Fitted for all phases	Fitted for all phases
FWHM (Cagliotti)/crystallite size for each phase	Fitted u, v, w independently for main phases and a common w for minor phases	Fitted u, v, w independently for main phases and a common w for minor phases	Fitted the crystallite size contribution	Fitted the crystallite size contribution
Iron content for $CaAl_{2-2x}Fe_{2x}O_4$ and $Ca_2Al_{2-y}Fe_yO_5$	x, y	Not significant	Fixed at $x=0.05$ and $y=0.5$	Not significant
Number of fitted parameters	~92	~92	~65	~65

Table 3
Agreement indexes obtained with each radiation for all samples

Sample	Synchrotron radiation diffraction					X-ray diffraction				
	R_{exp}	R_{wp}	R_p	χ^2	DW	R_{exp}	R_{wp}	R_p	χ^2	DW
A1	2.08	8.5	6.3	4.09	0.148	7.53	11.91	9.02	1.58	0.945
A2	2.07	8.18	5.99	3.94	0.149	7.29	11.65	8.99	1.6	0.885
A3	1.89	9.23	6.53	4.89	0.280	7.31	12.4	9.74	1.7	0.838
A4	2.08	9.71	7.07	4.68	0.113	7.34	13.86	10.76	1.89	0.620
A5	2.11	8.78	6.73	4.16	0.142	7.68	13.39	10.54	1.74	0.837
A6	1.61	9.21	6.75	5.71	0.099	7.47	12.72	9.91	1.7	0.733
A7	1.92	8.87	6.66	4.61	0.108	7.45	12.44	9.68	1.67	0.774
A8	2.07	8.49	6.46	4.1	0.144	7.66	12.08	9.41	1.58	0.888
A9	1.87	8.17	6.27	4.38	0.132	7.47	12.16	9.46	1.63	0.858
A10	2.2	9.52	6.97	4.32	0.144	7.37	13.53	10.48	1.84	0.635
B1	1.61	10.13	7.56	6.31	0.105	7.37	13.82	10.57	1.88	0.681
Nist1882	2.03	9.88	7.27	4.87	0.108	7.4	13.63	10.58	1.84	0.642
Std2	1.36	8.3	6.07	6.09	0.248	11.63	15.86	12.15	1.36	1.266
C1	2	11.06	7.69	5.52	0.078	7.33	14.64	11.2	2	0.584
C2	1.92	7.45	5.72	3.89	0.091	6.66	11.05	8.75	1.66	0.879
C3	2.19	10.55	7.44	4.81	0.188	6.53	10.54	7.99	1.61	1.001
D1	2.16	11.37	7.99	5.27	0.167	6.44	9.85	7.59	1.53	1.145
D2	2.12	10.29	7.16	4.85	0.195	6.43	10.04	7.79	1.56	1.094
D3	2.28	8.02	5.88	3.52	0.247	6.55	10.23	7.52	1.56	1.045
D4	2.33	8.05	5.67	3.45	0.288	6.49	10.03	7.99	1.55	1.114
D5	1.97	11.7	8.44	5.95	0.150	6.31	10.48	7.8	1.66	1.022
D6	2.13	8.13	5.9	3.82	0.219	6.43	10.18	7.53	1.58	0.980

(DW: Durbin–Watson statistics).

manufacturers, three from the E.U. and one from USA gave a positive answer, sending their samples. Ten samples, labeled A1 to A10 come from the same factory and are representative of the same product along a large historical period of the factory (about 40 years). Samples C1–C3, and D1–D6 belong to different products coming from two different manufacturers. Manufacturer B sent only one sample, B1. A synthetic mixture, STD2, was prepared mixing pure phases CA, $C_{12}A_7$, C_2AS, β-C_2S and C_4AF obtained by sintering the oxides ($CaCO_3$ for CaO) in platinum crucibles at an optimum temperature. A NIST1882 standard of this type of cement was also used. All the samples fall into two main groups: iron rich (up to 15% Fe_2O_3) and iron free. This latter group includes three subgroups: 1) low alumina-low iron group (C2), 2) medium alumina (70–75 wt.%, samples C3, D1,D2,D4,D5) and 3) high alumina (>80 wt.%, samples D3,D6).

2.2. Synchrotron X-ray powder diffraction (SXRD) measurements

All samples were received as powders, and all of them were manually passed through the agate mortar embedded in cyclohexane with the purpose of homogenize and disaggregate the powders, but avoiding to significantly reduce the crystallite size. The diffraction patterns were collected at the European Synchrotron Radiation Facility, beam line ID31, wavelength 0.495754 Å, equipped with a diffractometer in a Debye–Scherrer transmission configuration. Powder specimens were contained in a rotating borosilicate glass capillary, with diameter 1.5 mm and length 10 mm. Both wavelength and capillary diameter were chosen as a compromise between minimum absorption of the sample, and maximum representative volume. The sample analysis in capillary mode minimizes the preferred orientation of crystallites. The scan range was from 0° to 35° of 2θ at a speed of 0.75°/min, the intensity data was distributed in 0.002° steps, with resulting counting time of 0.16 s/step. The best FWMH (line breath) obtained with a LaB_6 diffraction standard was 0.01° of 2θ giving a resolution of ~0.016 Å, and the maximum diffracting intensity yield was $\sim 5 \cdot 10^6$ counts/s (NIST1882).

2.3. Conventional X-ray powder diffraction (XRD) measurements

Data were collected in a Siemens-D5000 powder diffractometer in a Bragg–Brentano geometry using CuK_α (1.540598+ 1.544426 Å) and a diffracted beam graphite monochromator. Samples were placed in a backmounted sample holder to minimize preferential orientation of the crystallites. The scan range was from 10° to 70° of 2θ, with step size of 0.02°, and measuring time 16 s/step. The best FWMH that can be obtained with the system of slit apertures used was ~0.1° of 2θ giving a resolution of ~0.07 Å, and the maximum diffracting intensity yield was $\sim 2 \cdot 10^3$ counts/s.

Table 4
Results obtained for synthetic sample STD2 analyzed with synchrotron radiation and X-ray in order to estimate the precision of the method

Phase composition		Sample STD2					Sample NIST 1882	
		Weighted	Wt.% Sync.	Rel. Dev.	Wt.% X-ray	Rel. Dev.	Wt.% X-ray	e.s.d.
$CaAl_{2-2x}Fe_{2x}O_4$	CA	62.5	62.5	0	62.7	−0.32	55.37	0.76
$Ca_{12}Al_{14}O_{33}$	$C_{12}A_7$	4.7	4.22	10.21	4.63	1.5	3.59	0.31
$Ca_2Al(Al,Si)O_7$	C_2AS	7.5	7.73	−3.06	9.18	−22.4	–	–
b-Ca_2SiO_4	b-C_2S	6.5	6.02	7.38	4.55	30.0	6.29	0.25
$Ca_2Al_{2-y}Fe_yO_5$	C_4AF	18.7	19.46	−4.06	17.55	6.15	20.38	0.57
$Ca_{20}Al_{26}Mg_3Si_3O_{68}$	Q	–	–	–	–	–	4.53	0.80
$CaTiO_3$	CT	–	–	–	–	–	1.54	0.17
$Ca_3Fe_2TiO_8$	C_3FT	–	–	–	–	–	5.57	0.36
FeO (wustite)	f	–	–	–	–	–	0.67	0.05
Fe_2O_3 (magnetite)	F	–	–	–	–	–	0.13	0.07
$Al(OH)_3$ (gibbsite)	AH_3	–	–	–	–	–	0.96	0.99
$Ca_3Al_2O_6 \cdot 6H_2O$	C_3A_{H6}	–	–	–	–	–	0.79	0.15

Mean results (five analysis) obtained for sample NIST 1882 analyzed with X-ray data in order to estimate the repeatibility of the method.

2.4. TG/DTA and chemical analyses

All the samples, except for the synthetic standard and NIST1882, were analyzed by X ray fluorescence (XRF). A 0.3 g portion of each sample was weighted and mixed with 5.7 g of $Li_2B_4O_7$ to obtain a 1/20 dilution. The homogenized mixture was transferred to a Pt crucible and melted to 1100 °C in a high frequency induction furnace. This method oxidizes all Fe to Fe_2O_3. Analyses were performed in a Philips 2400 X-ray spectrometer, and quantification was done by calibration of a group of 56 reference standards. Each sample was analyzed twice. The accurate chemical analyses of individual phases should be performed by electron microprobe (EMP) or by EDX-SEM on polished sections of clinker, see for instance [7]. However, in our case, these microanalytical techniques were not applicable, since we were only provided with powdered clinker samples.

These data were complemented by thermogravimetric/differential thermal analyses in order to obtain the loss of ignition and to

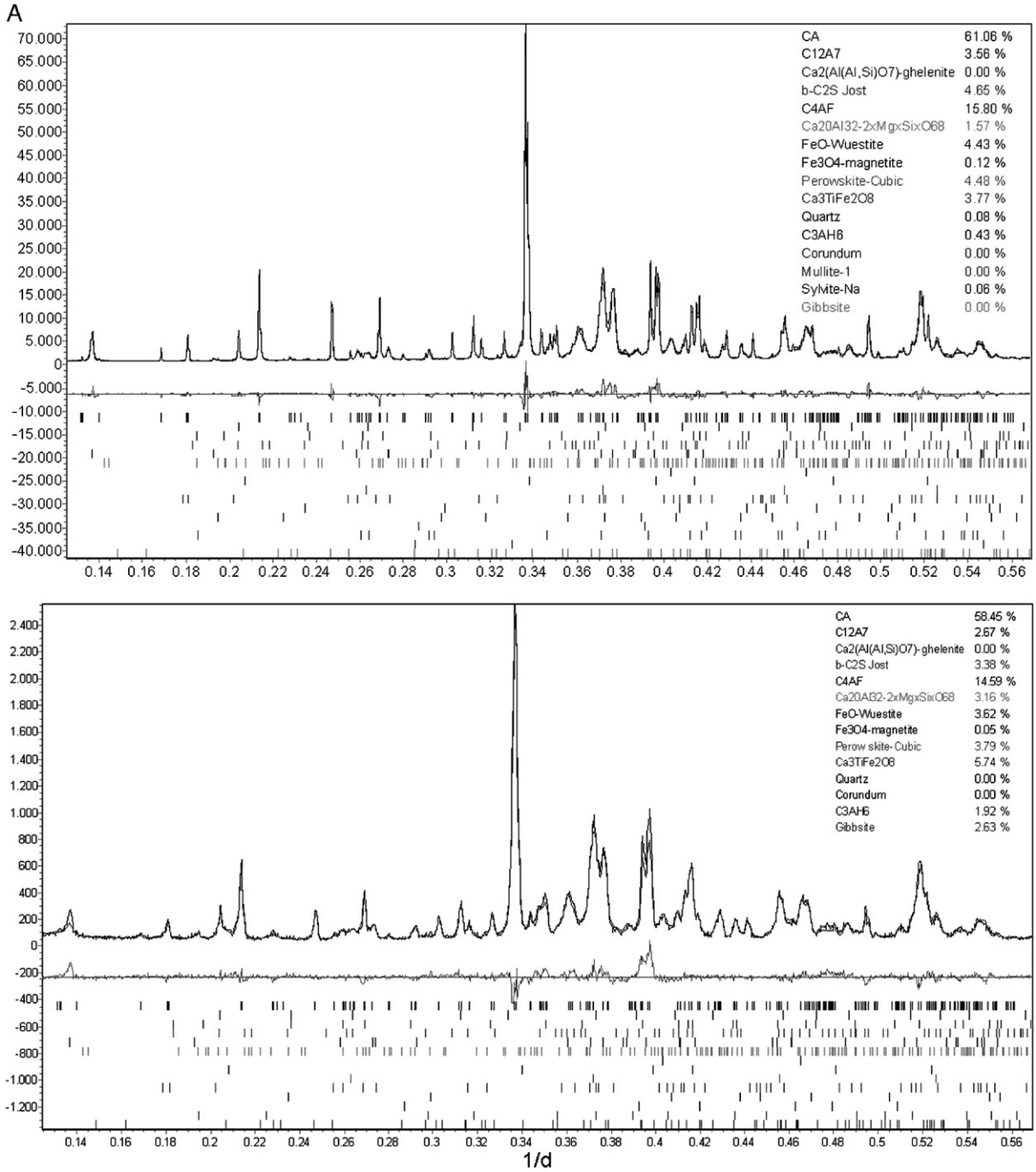

Fig. 1A. Observed, calculated and difference profiles, with quantitative results for each included phase. Diffractograms correspond to sample A9 (iron rich). Top profile corresponds to synchrotron data while bottom profile corresponds to conventional X-ray radiation. B. Observed, calculated and difference profiles, with quantitative results for each included phase. Diffractograms correspond to sample D3 (iron free). Top profile corresponds to synchrotron data while bottom profiles corresponds to conventional X-ray radiation.

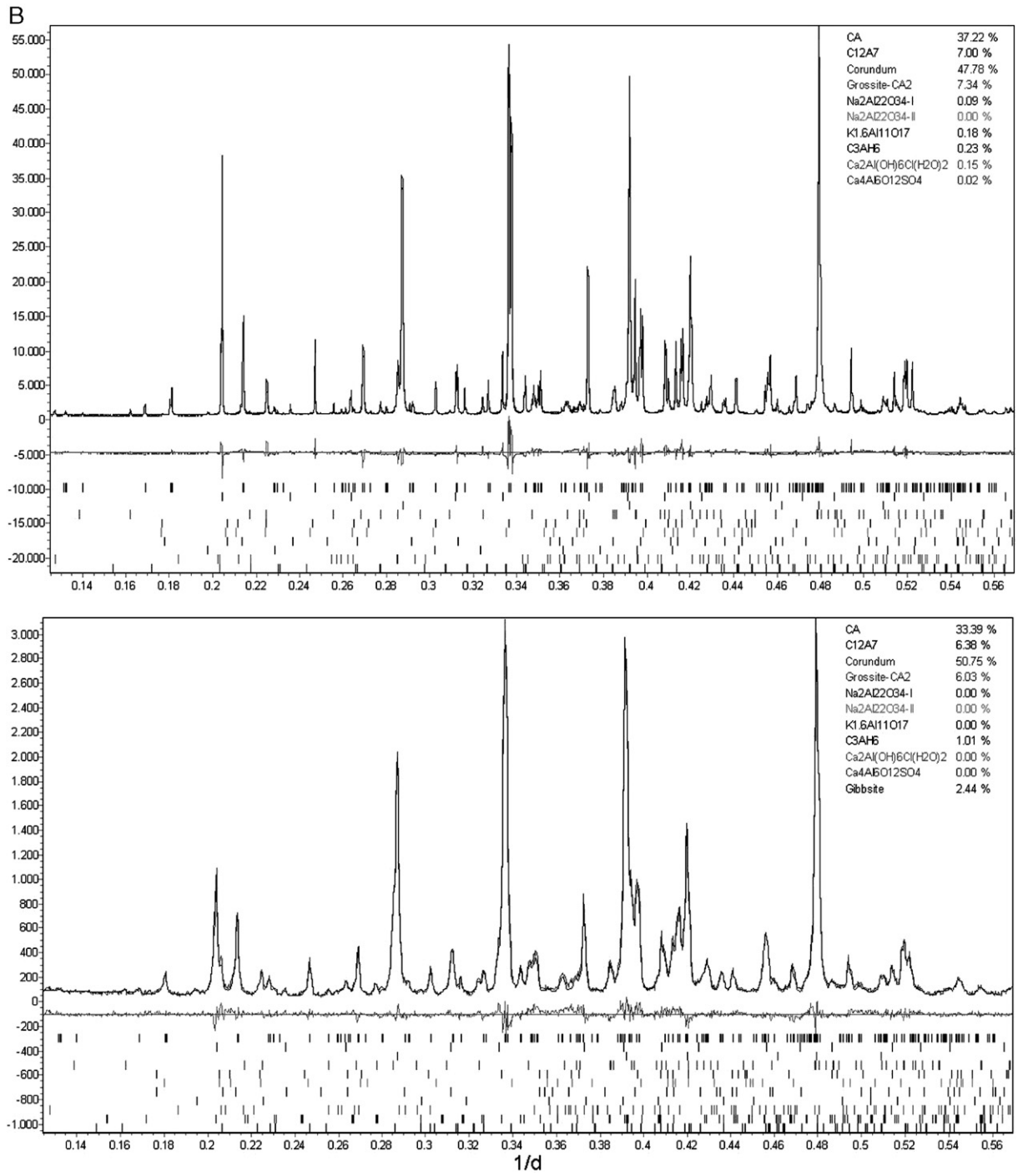

Fig. 1 (*continued*).

detect in the same analysis different types of water losses and oxidation/reduction effects. No tritration of water containing phases by KF-method was carried out. TG/DTA analyses were performed in a NETZSCH STA 409 C instrument between room and 1000 °C at 20 °C/min under air atmosphere. Reference material was alumina, and the weight of the samples were ~75 mg. Iron rich samples from factories "A" and "B", modify their weight with temperature in four well definite steps: between 100–200 °C and 200–350 °C there are two weight losses attributed to adsorbed water and dehydration of hydrated phases respectively; between 350–600 °C there is a weight increase for A and B samples due to oxidation of Fe, and between 600–750 °C a weight loss not clearly identified. Iron poor samples C2, C3 and D1–D6 always show the same two first weight losses, and C2 D1, D3 and D6 a third loss starting around 550 °C.

The composition of the samples, expressed in oxides, is given in Table 1. FeO content has been calculated on the basis of TG data. Lately, it will be shown that estimated FeO correlates well with the amount of wustite found by quantitative powder diffraction.

3. Results

3.1. Outline of the refinement procedure

Both synchrotron and conventional X-ray profiles were fitted using the computer program TOPAS 2.1 [13]. This program implements a wide variety of instrumental, profile and structural parameters and a robust convergence procedure, allowing a quick fit of complex multiphase crystalline systems. In spite of these advantages, there is some risk of fitting well (i.e. good agreement indexes) the experimental profile with a selection of unreliable parameters. The risk is higher for minor phases (less than ~3%), when high correlations between different parameters may occur. To save this drawback, the user is obliged to an accurate selection of the significant refined parameters, to avoid spurious correlations between parameters that can lead to biased quantitative results.

With X-ray data the so-called "fundamental parameters approach" [14] was used, with the obvious advantage of eliminating correlations between instrumental and sample plus crystallographic parameters. This approach takes the geometrical description of the diffractometer to calculate the instrumental contribution to diffracted profile. Consequently, only the sample contribution to profile is taken into account and refined (crystallite size and strain for each phase). Nevertheless, to fit the synchrotron data a classical pseudo-Voigt profile function and the FWHM description of Cagliotti [15] was used, because a parametric description of the instrument used at ESRF is not available at present.

After exhaustive tests carried on with different arrays of refinable parameters, we arrived to a choice, which is a compromise permitting a reliable estimation of the amounts of all identified phases in both kinds of calcium aluminate cements. The choice is different for synchrotron and conventional diffraction, the former permitting the identification of more phases and the refinement of a larger variety of parameters. In Table 2 the parameters used are summarized for synchrotron and conventional diffraction and for iron rich and iron poor cement.

The agreement indexes for all synchrotron and conventional diffraction refinement are given in Table 3. R_{exp}, R_{wp}, and R_p indexes are better for synchrotron refinements. The higher values obtained for the χ^2 statistics of synchrotron profiles, reflect the very high intensity yielded in synchrotron experiments: when the intensity data have been "over-collected", errors are not dominated by counting statistics anymore, R_{exp} will be very small and the ratio $\chi^2 = R_{exp}/R_{wp}$ larger than 1 [16]. This effect known as "serial correlation of data" is measured by the Durbin–Watson statistics that allows an interpretation of the deviation of χ^2 from the ideal value 1. Nevertheless, positive serial correlation has no effect on the accuracy of the refined parameters [17].

The accuracy of the method was estimated with standard STD2. Table 4 summarizes the results obtained for this sample with synchrotron radiation and X-ray. The precision for conventional X-ray diffraction was checked preparing and

Table 5
Phases used (grey color) in quantitative analysis for synchrotron and X-ray radiation and the two types of CAC

Phase composition		Database file		Synchrotron radiation diffraction		X-ray diffraction	
		ICSD	ICDD	Fe-rich cement	Fe-poor cement	Fe-rich cement	Fe-poor cement
$CaAl_{2-2x}Fe_{2x}O_4$	CA	260	70-134				
$Ca_{12}Al_{14}O_{33}$	$C_{12}A_7$	62040	78-910				
$Ca_2Al(Al,Si)O_7$	C_2AS	82706	35-755				
b-Ca_2SiO_4	b-C_2S	963	33-302				
$Ca_2Al_{2-y}Fe_yO_5$	C_4AF	9197	30-226				
$Ca_{20}Al_{26}Mg_3Si_3O_{68}$	Q	26353	74-695				
$CaTiO_3$	CT	31865	75-2100				
$Ca_3Fe_2TiO_8$	C_3FT	203100	84-2068				
FeO (wustite)	f	60683	46-1312				
Fe_3O_4 (magnetite)	F	20596	19-629				
$Al_2(Al_{2.5}Si_{1.5})O_{9.75}$	Mullite	202159	15-776				
SiO_2 (quartz)	S	41414	33-1161				
a-Al_2O_3 (corundum)	A	52025	43-1484				
$K_{0.7}Na_{0.3}Cl$	Silvite-Na	28941	26-920				
$CaAl_4O_7$	CA_2	16191	46-1475				
$NaAl_{11}O_{17}$		67545	21-1096				
$K_{1.7}Al_{11}O_{17}$		20117	84-380				
$Al(OH)_3$ (gibbsite)	AH_3	27698	33-18				
$Ca_3Al_2O_6\Sigma 6H_2O$	C_3AH_6	202315	38-368				
$Ca_2Al(OH)Cl(H_2O)_2$		62363	78-1219				
$Ca_4Al_6O_{12}SO_4$		80361	85-2210				

ICSD and ICDD database file numbers used for each phase are given.

analyzing five times the standard NIST 1882 (Table 4). In Fig. 1A and B selected examples of Rietveld refinement plots of synchrotron and conventional diffraction profiles are depicted.

3.2. Identification of "new" phases

The higher resolution and intensity of synchrotron data makes visible several phases that are not seen by conventional diffraction. Minor phases were identified by isolated peaks that appeared in synchroton data. Both diffraction peaks and mineralogical compatibility were the basis for accepting the occurrence of such minor phases. These discovered phases are only apparent by one or two small diffracting maxima, but introducing them in the refinement procedure improves the final agreement indexes. Suspected minor phases that were not represented by isolated non-overlapped peaks were not included in the refinement.

New phases may include minor oxides like magnetite, α-alumina, quartz, sodium or potassium chlorides coming from the production process itself and cement hydrated phases formed by contact of the clinker with the atmospheric moisture. For synchrotron data a total of sixteen phases were used for iron rich clinkers, while for iron free cement only ten phases are needed to simulate de experimental profile. Major and minor phases introduced in the refinements for synchrotron and conventional X-Ray data are given in Table 5. Quantitative results obtained from synchrotron data for all samples are depicted in Fig. 2.

The occurrence of such minor phases should be confirmed by other techniques such us selective dissolution [5,18], micro diffraction or electron diffraction. These techniques are far from the scope of this work, that tries to establish a model useful for on-line control in the production process of CAC.

3.3. Refinement of occupation factors in solid solutions

In the structures of CA and C_4AF, significant amounts of Fe^{+3} may substitute Al^{+3}. For CAC samples, the Fe/Al ratio cannot be established from XRD data because CA and C_4AF peaks are partially overlapped by other phases, and the resulting estimated error of the refined occupation factors is high. This is the reason why, for XRD data, the occupations of Fe^{+3} and Al^{+3}

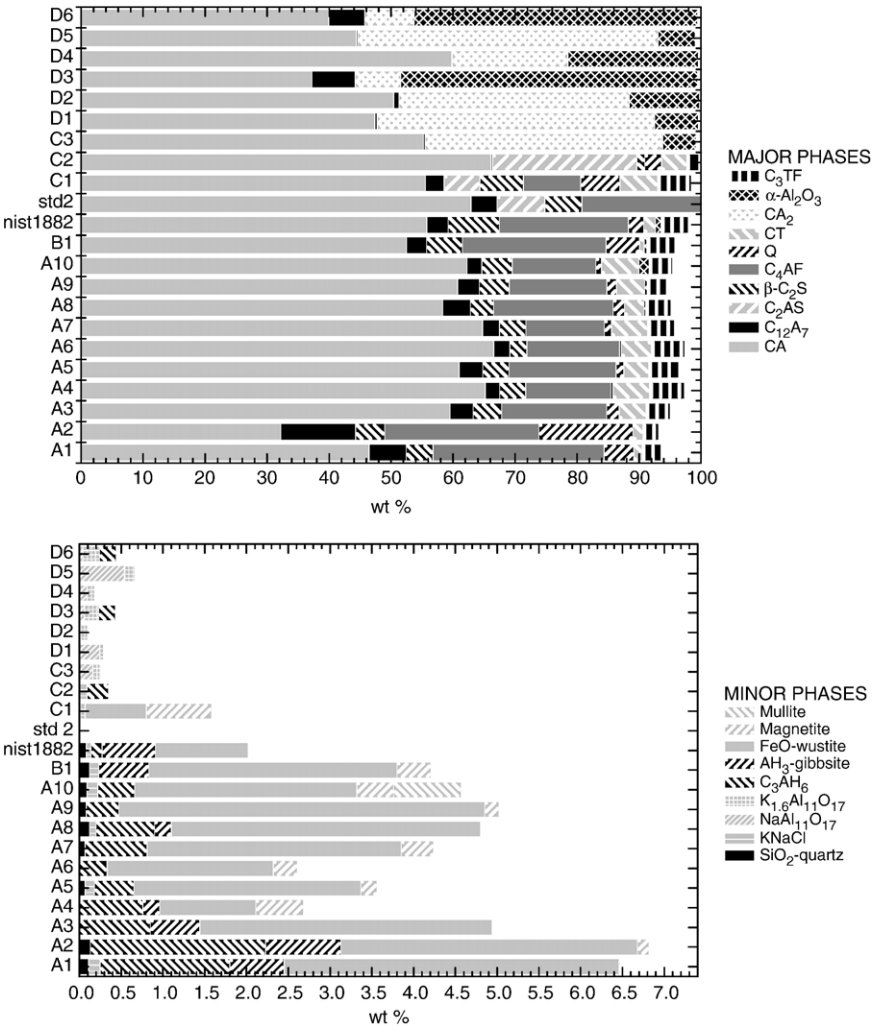

Fig. 2. Quantitative results from synchrotron data obtained for all samples. Top figure summarizes major phases whereas the bottom one summarizes the minor phases.

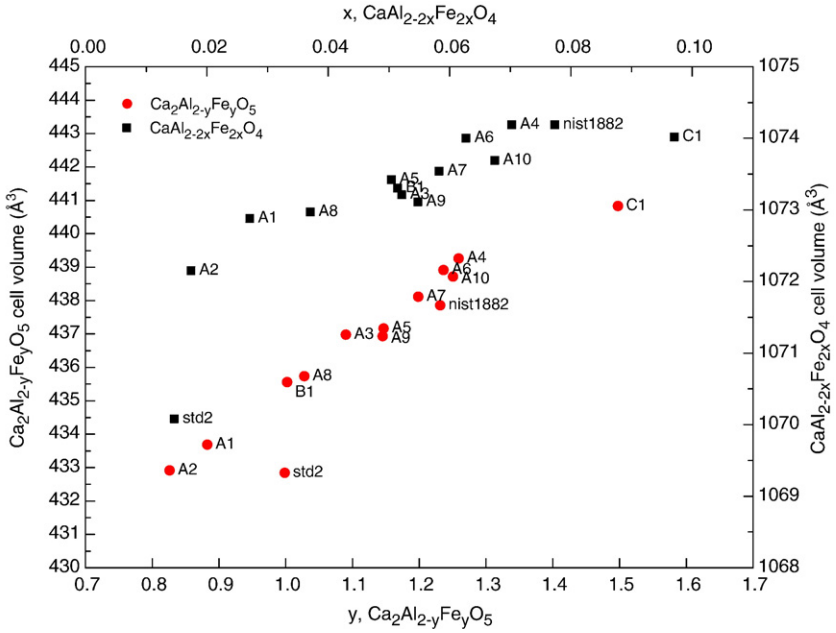

Fig. 3. Iron content for $CaAl_{2-2x}Fe_{2x}O4$ (■) and $Ca_2Al_{2-y}Fe_yO_5$ (●) solid solutions (calculated from the refined Fe^{+3} occupation factor in these structures) plotted against the cell volumes (calculated from the refined cell parameters).

are fixed to a value previously investigated, or based in general crystallochemical considerations [9,10]. For the CA phase the fixed Fe/Al ratio is more accurate than for C_4AF, because in the latter, Fe^{+3} can be substituted by other cations different from Al^{+3} [19]. With SXRD profiles, the cation occupation of these sites is refined, but constrained by a minimum and maximum possible values. The iron content in the above phases has important influence on the distribution of phases in the sample. Other cation substitutions in minor phases (i.e. substitution of silicon by phosphor in β-C_2S, [20] Ti^{+4} in C_4AF or Ti^{+4} by Si^{+4} in perovskites [21]) were not investigated. In Fig. 3 Fe^{+3} occupation factors in CA and C_4AF are plotted against the cell volumes calculated from the refined cell parameters of the same phases. Solid solutions for iron free CACs are not significant, and were not taken into account.

3.4. Comparison between quantitative SXRD and XRD results

One aim of this work was to validate XRD results by comparing them with those obtained with a more powerful and reliable tools as SXRD. Synchrotron results are taken as the best reference for evaluating the quality of quantitative results obtained from conventional data. In Fig. 4 quantitative results for major and minor phases obtained by synchrotron are plotted against the relative deviation between XRD and SXRD given by the

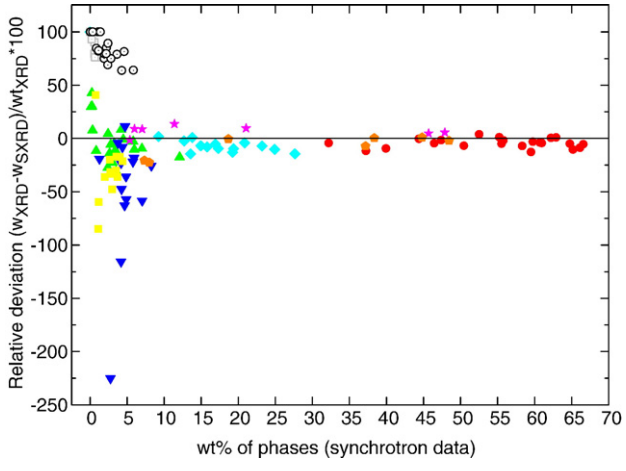

Fig. 4. Quantitative results obtained for each phase from synchrotron data plotted against the relative deviation of the same value calculated from X-ray data $[(wt_{xrd} - wt_{sxrd})/wt_{xrd} * 100]$.● CA,▲ $C_{12}A_7$, ▼β–C_2S,◆ C_4AF,■ A,CA_2, ○ C_3AH_6, □ AH_3.

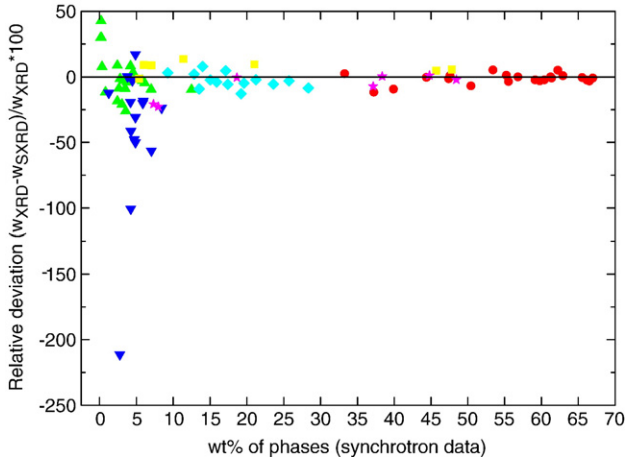

Fig. 5. Quantitative results obtained for each phase from synchrotron data plotted against the relative deviation of the same value calculated from X-ray data $[(w_{XRD} - w_{SXRD})/w_{XRD} * 100]$. In these calculations both minor and hydrated phases were excluded from the refinement.●CA,▲ $C_{12}A_7$,▼ β-C_2S,◆ C_4AF,■ A,★ CA_2.

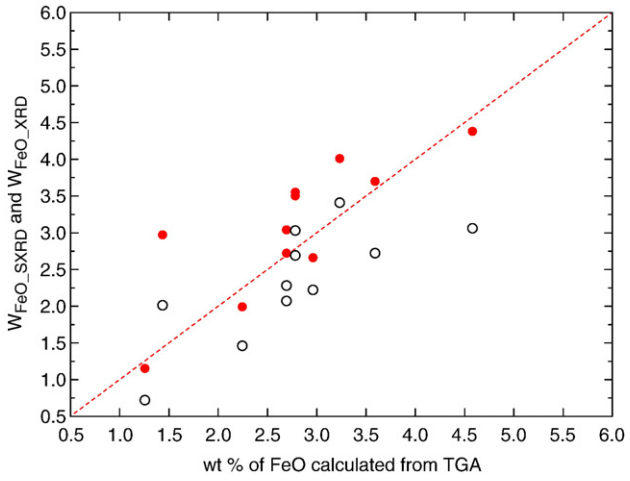

Fig. 6. Weight percent of FeO obtained by quantitative diffraction plotted against the amount of FeO estimated by thermogravimetry (●SXRD, ○ XRD).

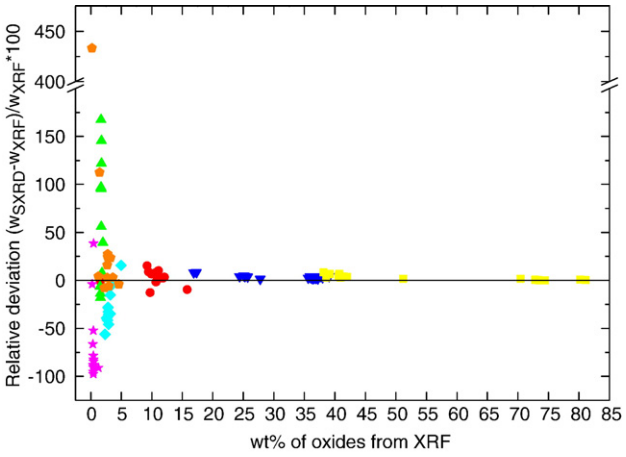

Fig. 8. Quantitative results of pure oxides obtained from XRF analysis and TGA (FeO) plotted against the relative deviation of the same value calculated back from quantitative phase analysis with synchrotron data [($w_{SXRD}-w_{XRF}$)/w_{XRF}*100]. ● Fe_2O_3, ▲ TiO_2, ▼ CaO, ◆, SiO_2, ■ Al_2O_3, ⬟ FeO, ★MgO.

expression $((W_{XRD}-W_{SXRD})/W_{XRD})\cdot 100$. Significant deviations from the reference ideal line are seen for high and low absorbing phases. Fig. 4 may be compared with Fig. 5, representing quantitative results obtained when minor and hydrated phases are excluded from the refinements. It is apparent that the exclusion of minor phases do not change significantly the results.

3.5. Obtention of the ratio Fe^{+2}/Fe^{+3}

For iron bearing CACs, the Fe^{+2}/Fe^{+3} ratio may give useful information on the operating conditions of the furnace, and has some influence on the distribution of phases in the clinker and final hydraulic properties of the cement. Assuming that all iron Fe^{+3} is located in the structures of CA, C_4AF C_3FT and magnetite, and Fe^{+2} crystallizes as wustite and is included in magnetite, Fe^{+2}/Fe^{+3} ratio may be easily estimated. In Fig. 6 the weight percent of FeO obtained by quantitative diffraction from both, synchrotron and conventional data is compared with the amount of FeO estimated by thermogravimetry. Fe^{+2} can be bound to pleochroite as well, but its inclusion in this phase would not change significantly the overall quantitative results for Fe^{+2}, but, on the other hand, it would reduce even more the total amount of estimated MgO in the sample. Provided that pleochroite was the most important Mg bearing phase, it was preferred, for the sake of simplicity, to introduce a fixed composition $Ca_{20}Al_{26}Mg_3Si_3O_{68}$ for this mineral [22]. In addition, pleochroite occurs as a mixed layer intergrowths with ghelenite [23], making the estimation of Fe^{+2}/Mg more problematic.

3.6. Comparison between the estimated weight percent of hydrated phases and the loss of ignition (l.o.i.)

As stated above, the weight loses on heating are produced mainly in three steps between 100–200, 200–350 and 600–1000 °C. An indirect proof of the reliability of quantitative results regarding the hydrated phases can be obtained by

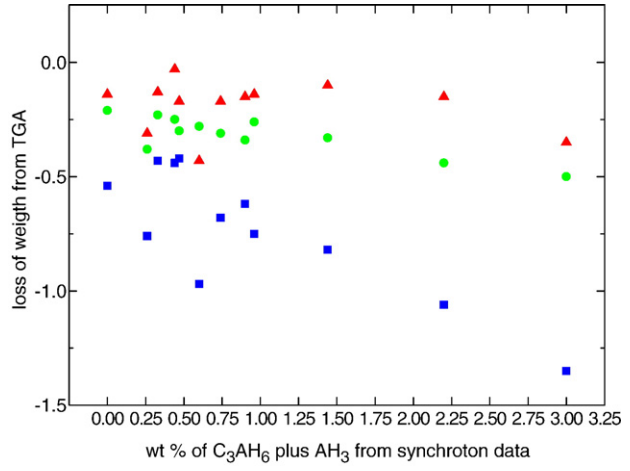

Fig. 7. Quantitative results of hydrated phases (AH_3 plus C_3AH_6) calculated from synchrotron data plotted against the three weight loses observed by TGA: first at 100–200 °C (●), second at 200–350 °C (■) and third at 600–1000 °C (▲).

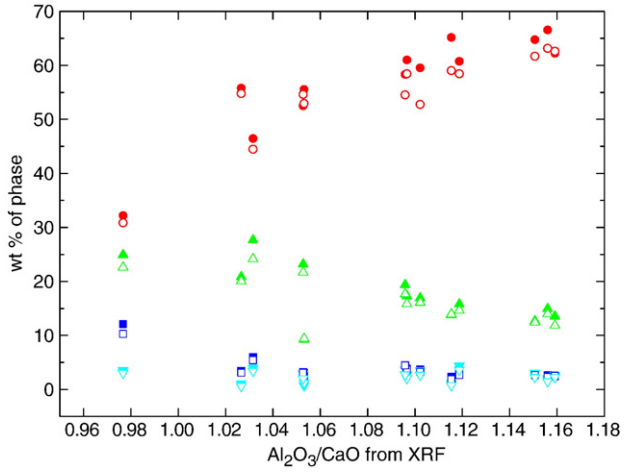

Fig. 9. Relationships between the amounts obtained for main phases and Al_2O_3/CaO ratios from XRF. Filled symbol corresponds to SXRD whereas opened symbol corresponds to XRD: ●, ○ CA; ■, □ $C_{12}A_7$; ▲, △ C_4AF; ▼, ▽ FeO; ◆.

plotting the weight percent of these phases against each step of the l.o.i. It can be observed in Fig. 7 that a clear correlation exists between quantitative values for C_3AH_6 plus AH_3 and the second step of l.o.i., between 200–350 °C.

3.7. Comparison between XRF analysis and calculated oxides based on quantitative diffraction

Accurate results of quantitative Rietveld analysis should return the correct composition of the sample, provided two conditions are fulfilled: the fraction of amorphous phase in the sample is negligible, and the solid solutions are correctly described by the refined occupation factors. CAC samples do not present polymorphic pairs of phases, so that all phases bear different compositions: increasing the weight percent of a given phase automatically increases the weight percent of its components and reduces the remainder ones. Hence, calculating back the composition from quantitative diffraction and comparing the results with those obtained by chemical analysis is a convenient test of the accuracy of the Rietveld quantitative method. In Fig. 8, the calculated weight percent of CaO, Al_2O_3, Fe_2O_3, FeO, SiO_2, TiO_2 and MgO are compared with XRF analysis (except for Fe_2O_3/FeO, estimated through TG).

4. Discussion

4.1. Refinement procedure

For quantitative Rietveld analysis of a multiphase sample, the refined scale factor of phase α, S_α, is the main determining parameter of the weight fraction of each phase α, W_α through the known relation [24]:

$$W_\alpha = \frac{S_\alpha \cdot (ZMV)_\alpha}{\sum_{\alpha=1}^{n} S_\alpha \cdot (ZMV)_\alpha}$$

where Z, M, V are the numbers of formula unit per unit cell, mass of the formula unit and unit cell volume of phase α in a mixture of n phases. The scale factor is correlated with other parameters describing the profile or the structure of different phases. Several correlations are undesirable in the sense that may lead to biased quantitative results. A fundamental part of this work consisted in finding a selection of suitable profile and structural parameters for each kind of CAC samples. A wise selection should take into account two basic rules: a) include the minimum number of parameters needed for the fit, and b) the parameters should have a defined physical meaning. To accomplish the second rule it was necessary to constrain the cell parameters, the occupation factors and peak breadths of all phases to reliable values. The CAC rich in iron presents several solid solutions that can modify significantly the cell parameters. On the other hand, this type of cement includes phases of low crystallinity reflected by wide peaks in the diffractogram.

Examples of important correlations are, for minor phases, the link between S_α and the breath of diffraction peaks or the background. For major solid solution phases, S_α may correlate with the occupation factors of crystallographic positions filled with different chemical species. In addition, occupation factors modify the molecular weight, influencing directly W_α.

In summary, the detailed crystallographic characterization of phases present in CACs carried out in recent years, together with the knowledge of the physical parameters describing the instrumental profile, reduce the number of parameters to be refined and hence the undesired correlations between them.

4.2. Accuracy and precision of the results

The accuracy may be tested by comparing the weighted phases of synthetic mixtures with the calculated weights obtained by the refinement. For major phases (more than 15% by weight), the relative percent error obtained by synchrotron data ranges from 0.0% to 4% or from 0.3% to 6% when conventional diffraction is used. For intermediate phases, deviation may attain up to 30% for conventional X-rays. Finally, very minor phases may deviate by more than 100%. In these phases, the accuracy depends on the occurrence of isolated peaks, which is highly contingent, since it is influenced by the relative amounts of all remainder phases. Frequently, minor phases concentrate a given minor chemical component (i.e. wustite, FeO; larnite, SiO_2). In this case, comparison between chemical and diffraction results may help in the estimation of the deviation. Another factor producing systematic deviations is the absorption contrast between phases. Less absorbing phases (i.e. hydrates) are overestimated, while the more absorbing ones are underestimated. This effect is more pronounced for softer radiations (in our case, conventional X-rays) and minor phases. However, there is not a simple relation between deviations of estimated weight fractions and the corresponding linear absorption coefficient. For instance, larnite is always more underestimated than wustite, even if its linear absorption coefficient is much lower. Until a simple relation between these variables is found, it will be

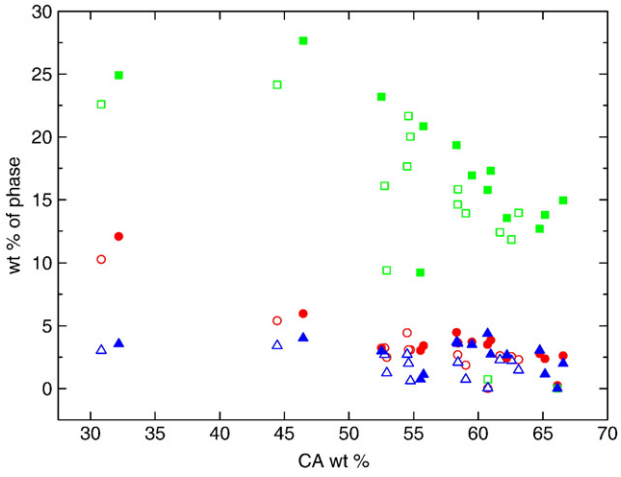

Fig. 10. Relationships between the amounts obtained for CA and $C_{12}A_7$ (●, ○), C_4AF (■, □) and FeO (▲, △). Filled symbol corresponds to SXRD whereas opened symbol corresponds to XRD.

necessary to apply empirical factors, such those that can be easily deduced from Fig. 4.

The presence of an amorphous phase in the clinker is an intrinsic limitation of the standardless Rietveld quantitative analyses. Diffraction maxima are only given by crystalline phases. Amorphous or non-crystalline phases are characterized by a smooth maximum emerging from the background. For simple diffractograms, it is possible in principle to identify the presence of an amorphous phase, but for complex samples, the amorphous hill is usually immersed by the multiple overlapping of the tails of neighbouring peaks. When refining the background, the amorphous phase is systematically excluded. Another limitation of the method are the minor crystalline phases not included in the refinement (for synchrotron, less than ~0.5–1%). Since the weights of the phases included are constrained to 100%, these weights are always overestimated by an imprecise amount. Altogether, amorphous plus non-included minor phases may represent up to a 5% by weight in conventional diffraction [4]. A point to bear in mind is that the amorphous phase may concentrate a high percent of the silica of the sample.

Powder diffraction experiments with clinker are highly reproducible if all steps are fulfilled according to an exact routine (Table 4). The most variable step is the specimen preparation, in special when flat specimens are prepared by hand. Whenever comparative results are needed, for instance, performing routine quality control in a factory, it is advisable to find an automatic procedure for mounting the specimen powders in the holder. Measurements of 5 independent sample preparation led to determination of the values for accuracy and precision for X-ray data. Our measurements agree well with previous results [18,25].

4.3. Chemical composition calculated from quantitative diffraction

For iron free CACs, the agreement between calculated and analysed oxides can be considered excellent, for both sinchrotron and X-ray cases. This can be corroborated by comparing Fig. 8 (see contents of Al_2O_3 and CaO greater than 50% and lesser than 35% respectively), with Table 1. For these simple compositions we may conclude that estimated weight fractions of clinker phases are highly accurate.

Iron bearing CACs have a more complex composition and they include more phases. In particular, these CACs usually contain an amorphous phase that can not be quantified without the addition of a standard. The exclusion of non-refinable phases will result in an overestimation of the major components of major phases, i.e. Al_2O_3 and CaO (see Fig. 8).

Minor oxides as SiO_2, TiO_2, etc. are concentrated in minor phases. SiO_2 is always underestimated : first of all, larnite, the most important silica bearing phase is underestimated by quantitative diffraction as stated above, and secondly, the amorphous phase is suggested to be richer in silica. For TiO_2, one source of positive deviation is the systematic overestimation of C_3TF, and a secondary source of error could be the substitution of Ti^{+4} by Si^{+4} in perovskite CT [21].

4.4. Useful correlations

Several comparative tests were performed with the aim of ascertaining that conventional Rietveld method is fully reliable for the quantification of major and intermediate phases. For iron rich CACs there are several relationships between phases themselves, and between phases and composition, that have important meanings with regards the conditions of the manufacturing process, crystallization of minerals and finally the setting and strength properties of the material. These are relationships between the amounts of phases and Al_2O_3/CaO ratios [26], (Fig. 9), and relationships between C_4AF, $C_{12}A_7$ and wustite and the CA phases (Fig. 10). It can be observed that the trends obtained by sinchrotron and conventional XRD are similar and foreseeable, indicating that conventional XRD results are as reliable as those obtained from synchrotron radiation whenever major phases are examined.

5. Conclusions

Compared with conventional powder diffraction, SXRD greatly improves the intensity and resolution of powder diffraction profiles, permitting the identification of new minor phases not observed before by DRX.

The solid solutions present in iron rich CACs are better characterized by SXRD.

The SXRD minimizes the effects of preferred orientation of crystallites and reduces the microabsorbtion of X-rays by the sample.

As a result, SXRD improves the accuracy of the quantification of phases in CACs, and hence it can be used as a reference test for assessing the accuracy of quantitative results obtained by conventional XRD.

The comparison between SXRD and XRD Rietveld refinements, permits to find the best selection of profile and structural parameters to be refined in conventional XRD. In particular, the "fundamental parameters approach" has been demonstrated to minimize the undesirable correlations between profile and structure parameters, and is highly advisable whenever a great number of phases are to be quantified.

For major and intermediate phases, the quantitative results obtained from conventional powder diffraction are comparable to those obtained by SXRD, when a wise selection of refined parameters are implemented. Therefore, conventional XRD Rietveld quantitative analysis is confirmed as a reliable, straightforward tool in CACs cement industry.

A minor common drawback to both SXRD and XRD is the systematic underestimation of larnite. This is reflected in the calculated composition of iron rich CACs by a depletion of the SiO_2 component, which is influenced as well by the exclusion of the glass phase from quantitative diffraction analyses.

Acknowledgements

We thank the anonymous providers of the CACs samples that permitted us to carry out this work, Bruker AXS for facilitating a free access to the TOPAS software, and ESRF for the provision of synchrotron facilities (Invitation for Experiment number CH-

1507). We also thank Dr. M.A. García Aranda for his assistance in the SXRD experiments. This study received financial support from the Spanish Government, project MAT2001-3345.

References

[1] J.C. Taylor, I. Hinczak, C.E. Matulis, Rietveld full-profile quantification of Portland cement clinker: the importance of including a full crystallography of the major phase polymorphs, Powder Diffr. 15 (1) (March 2000) 7–18.
[2] A.G. de la Torre, A. Cabeza, A. Calvente, S. Bruque, M.A.G. Aranda, Full phase analysis of Portland clinker by penetrating synchrotron powder diffraction, Anal. Chem. 73 (2001) 151–156.
[3] T. Füllmann, G. Walenta, T. Bier, B. Espinosa, K.L. Scrivener, Quantitative Rietveld phase analysis of calcium aluminate cements, World Cem. Res. (June 1999) 91–96.
[4] F. Guirado, S. Galí, S. Chinchón, Quantitative Rietveld analysis of aluminous cement clinker phases, Cem. Concr. Res. 30 (2000) 1023–1029.
[5] H. Motzet, H. Poellman, Quantitative phase analysis of high alumina cements, ICMA, Guadalajara, Mexico, 1998, pp. 187–206.
[6] H. Pöllmann, Mineralogy and crystal chemistry of calcium aluminate cement, Proceedings of Int. Conf. On Calcium Aluminate Cements, Edimburg, 2001, pp. 79–119.
[7] B. Touzo, A. Gloter, K.L. Scrivener, Mineralogical composition of Fondu revisited, Proceedings of Int. Conf. On Calcium Aluminate Cements, Edimburg, 2001, pp. 129–138.
[8] F.P. Sorrentino, F.P. Glasser, Crystallization of $CaO–Fe_2O_3–Al_2O_3–SiO_2$, Trans. Br. Ceram. Soc. 74 (1975) 253–265.
[9] F. Guirado, S. Galí, J.S. Chinchón, The crystallography of $CA_{1-x}F_x$ using X-ray powder diffraction techniques, Cem. Concr. Res. 24 (5) (1994) 923–930.
[10] F. Guirado, S. Galí, J.S. Chinchón, X-ray profile analysis of $Ca_2Fe_{2-x}Al_xO_5$, World Cem. 27 (12) (1996) 73–76.
[11] H.P. Klug, L.E. Alexander, X-ray diffraction procedures, John Wiley and Sons, New York, 1962.
[12] L.W. Finger, Synchrotron powder diffraction, in Modern Powder Diffraction, in: D.L. Bish, J.E. Post (Eds.), Mineralogical Society of America, 1989.
[13] TOPAS, General Profile and Structure Analysis Software for Powder Diffraction Data, V2.1, Bruker AXS Gmbh, Karlsruhe, Germany.
[14] R.W. Cheary, A.A. Coelho, A fundamental parameter approach of X-ray line-profile fitting, J. Appl. Crystallogr. 25 (1992) 109–121.
[15] G. Cagliotti, A. Paoletti, F.P. Ricci, Choice of collimators for a crystal spectrometer for neutron diffraction, Nucl. Instrum. Methods 3 (1958) 223–226.
[16] L.W. MacCusker, R.B. Von Dreele, D.E. Cox, D. Louër, P. Scardi, Rietveld refinements guidelines, J. Appl. Crystallogr. 32 (1999) 36–50.
[17] R.J. Hill, I.C. Madsen, The effect of profile step width on the determination of crystal structure parameters and estimated standard deviations by X-ray Rietveld analysis, J. Appl. Crystallogr. 19 (1986) 10–18.
[18] F. Goetz-Neunhoeffer, Quantitative phase analysis of various Fe-rich calcium aluminate cement clinkers by selective dissolution and XRPD, Proceedings of the 11th Int. Cong. On the Chem. of Cement, Durban, South Africa, 2003, pp. 125–133.
[19] B. Touzo, A. Gloter, K. Scrivener, T. Füllmann, G. Walenta, Phase composition of 40% Al_2O_3 calcium aluminate cements, Proceedings of the 11th Int. Cong. On the Chem. of Cement, Durban, South Africa, 2003, pp. 1931–1940.
[20] R. Müller, J. Neubauer, F. Götz-Neunhofer, Effects of phosphate rich raw materials on the crystallographic and hydraulic properties of dicalcium silicate, Proceedings of the 11th Int. Cong. On the Chem. of Cement, Durban, South Africa, 2003, pp. 1045–1053.
[21] B. Touzo, A. Gloter, K.L. Scrivener, Mineralogical composition of Fondu revisited, Proceedings of Int. Conf. On Calcium Aluminate Cements, Edimburg, 2001, pp. 129–138.
[22] F. Hanic, M. Handlovic, I. Kapralik, The structures of a quaternary phase $Ca_{20}Al_{32-2x}Mg_xSi_xO_{68}$, Acta Crystallogr. 336 (1980) 2863–2869.
[23] A. Sourie, F.P. Glasser, E.E. Lachowski, Microstructural studies on pleochroite, Br. Ceram. Trans. 93–2 (1994) 41–48.
[24] D.L. Bish, S.A. Howard, Quantitative phase analysis using the Rietveld method, J. Appl. Crystallogr. 21 (1988) 86–91.
[25] A.G. De la Torre, M.A.G. Aranda, Accuracy in Rietveld quantitative phase analysis of Portland cements, J. Appl. Crystallogr. 36 (2003) 1169–1176.
[26] K.W. Harr, Relationship between mineral phases C4AF and CA in calcium aluminate cements with high iron content, Proceedings of Int. Conf. On Calcium Aluminate Cements, Edimburg, 2001, pp. 121–127.